A&A manuscript no.
(will be inserted by hand later)

Your thesaurus codes are:
08 (08.01.1; 08.01.3; 08.13.2; 08.23.2)

ASTRONOMY
AND
ASTROPHYSICS
27.1.1995

Spectral analyses of 25 Galactic Wolf-Rayet stars of the carbon sequence

L. Koesterke and W.-R. Hamann

Institut für Theoretische Physik und Sternwarte der Universität, D-24098 Kiel, Federal Republic of Germany,
e-mail: (L.K.) pas19@rz.uni-kiel.d400.de

Received date; accepted date

Abstract. We present a grid of helium-carbon models for Wolf-Rayet (WR) stars of the carbon sequence (WC) with $\beta_C = 0.2$ (carbon mass fraction), thus extending our previously released grid with $\beta_C = 0.6$ to a different chemical composition. The WR model atmospheres are based on the so-called standard assumptions. The calculations account for non-LTE radiation transfer in spherically expanding atmospheres. Helium and carbon are represented by detailed model atoms, especially concerning the ions C III and C IV.

Using the model grids 25 Galactic WC stars of intermediate subtype (WC 5 to WC 8) are analyzed. Subsequently we perform fine analyses by calculating several individual models for each of the program stars. Temperatures, radii, mass-loss rates and terminal velocities are determined together with the carbon to helium ratio.

The analyzed WC stars are found to form two groups, which can be distinguished by the strength of their emission lines. Stars with weak lines (WC-w) have effective temperatures close to 50 kK and their winds are relatively thin, forming the continuous spectrum in regions with small expansion velocities. WC stars with strong lines (WC-s) have higher effective temperatures (60 to 100 kK, referring to the core radius) and thick winds. Thus there is a strong analogy to the distribution of the early-type WN stars (WNE-w and WNE-s, respectively). For the WC stars we determine luminosities between $10^{4.7}$ and $10^{5.5}\,L_\odot$ and mass-loss rates from $10^{-4.8}$ to $10^{-3.9}\,M_\odot\,\mathrm{yr}^{-1}$. The carbon mass fraction varies from 0.2 to 0.6. No correlation is found between the carbon abundance and any of the stellar parameters (e.g. temperature, luminosity) or the spectral subtype.

The evolution of WR stars is discussed by comparing the results of our analyses with evolutionary tracks.

Key words: stars: Wolf-Rayet – stars: atmospheres – stars: abundances – stars: mass-loss

Send offprint requests to: L. Koesterke

1. Introduction

For a better understanding of the role of carbon-type Wolf-Rayet stars (WC) in the scenario of stellar evolution their effective temperatures, luminosities, mass-loss rates and chemical compositions must be determined. Because appropriate model calculations have been lacking for a long time, this field of work is still in its infancy. Black-body continua and one-point models in Sobolev approximation are inadequate. In the recent years program codes, accounting for the very complex physical conditions in WR atmospheres, have been developed (Wessolowski et al. 1988; Hillier 1988, 1989) which allow the synthesis of continua and emission line spectra. They have been successfully applied to WR stars of both the nitrogen (WN) and the carbon (WC) sequence.

The WN stars have been studied comprehensively taking advantage of the dominance of helium in their atmospheres (Schmutz et al. 1989, Hamann et al. 1993, Hamann et al. 1994, Crowther et al. 1994a,b). The fundamental stellar parameters (effective temperatures, radii, mass-loss rates, terminal velocities, hydrogen abundances) for an almost complete Galactic WN sample have been determined (Hamann et al. 1994).

Because of the more complex chemical composition of WC stars, pure-helium models are insufficient and at least carbon must be taken into consideration. Two pilot studies both investigating the WC 5 star WR 111 (alias HD 165763) have been published (Hillier 1989; Hamann et al. 1992). Furthermore one grid of helium-carbon models has been established (Koesterke et al. 1992) for a fixed carbon to helium ratio of 60:40 (by mass). The present work is based on these preparatory studies and is a step towards a comprehensive analysis of the Galactic WC sample.

The present study is restricted to the intermediate subtypes (WC 5-WC 7) for which the applied models are most suitable. Models for early subtypes (WC 4 and WO) would require the inclusion of oxygen, while the low ionisation stages of carbon (C II) must be accounted for in more detail in WC 9 and later. Note that the WC sequence (WC 4 to WC 10) is continued towards "earlier" subtypes by the WO sequence (Barlow & Hummer 1982).

The analyses proceed in two steps. First the stellar parameters, including the carbon abundances, are determined from comparing the measured equivalent widths of several helium and carbon lines with the model grids (coarse analysis). Subsequently, for each individual star, several models are calculated and line profile fits are performed (fine analysis). Particular care is taken in determining the carbon abundance.

In Sect. 2 we briefly characterize the model atmospheres. In Sects. 3 and 4 we present the model grid and the observational data, respectively. In Sect. 5 the coarse analyses are described, while some modifications are tested in Sect. 6. Sect. 7 contains the description of the fine analyses. A summary of the results and a discussion of the evolutionary status is given in Sect. 8.

Table 1. Parameters of the model grids

fixed:				
$\beta_{\rm C}$	(mass fraction)	0.6 & 0.2		
v_∞	[km s^{-1}]	1800		
$\dot{M}$	[$M_\odot$ yr^{-1}]	$10^{-4.0}$		
varied:				
T_*	[kK]	31.6	...	100
R_*	[$R_\odot$]	1.6	...	50
$R_{\rm t}$	[$R_\odot$]	1.3	...	40

2. Model atmospheres

The model calculations are very similar to those described in Koesterke et al. (1992). They are based on the standard assumption of a spherically symmetric, homogeneous and stationary flow. Each WC model is specified by the five basic parameters effective temperature T_*, stellar radius R_*, mass-loss rate $\dot{M}$, terminal velocity v_∞ and carbon abundance $\beta_{\rm C}$. The exponent of the analytic velocity law is set to $\beta = 1$ and a microturbulence of $v_{\rm D} = 100\,{\rm km\,s^{-1}}$ is assumed. The introduction of the transformed radius $R_{\rm t}$ by the transformation law

$$R_{\rm t} = R_* \left[\frac{v_\infty}{2500\,{\rm km\,s^{-1}}} \Big/ \frac{\dot{M}}{10^{-4}\,M_\odot\,{\rm yr^{-1}}} \right]^{2/3} \qquad (1)$$

reduces the number of independent parameters, because models with the same T_*, $R_{\rm t}$ and $\beta_{\rm C}$ show very similar synthetic spectra, i.e. the equivalent widths of the emission lines are nearly the same (cf. Hamann et al. 1992). The coarse analysis technique, introduced by Schmutz et al. (1989) for WN stars and extended to WC stars by Koesterke et al. (1992), is founded on this fact.

To facilitate the analysis we established a second grid of helium-carbon models which covers the same range of stellar parameters as the one presented previously (Koesterke et al. 1992), but with a lower carbon abundance of $\beta_{\rm C} = 0.2$ instead of $\beta_{\rm C} = 0.6$ (cf. Table 1). The two grids are prerequisite for the coarse analyses (Sect. 5). To obtain consistent grids we have used nearly the same model atom as in Koesterke et al. (1992), but two improvements in the atomic model, affecting the C III lines at 1909 Å and 6742 Å (cf. Koesterke et al. 1992), have been corrected. The intercombination transition at 1909 Å is now treated explicitely in the Co-Moving-Frame formalism and not in an optically thin approximation as we usually do with forbidden lines. The other C III line, at 6742 Å, is now calculated with an improved branching ratio for the three most important transitions from the $2p3p\,^3D$ state (calculated by Storey, unpublished, but quoted by Hillier 1991), but the exact strength of C III 6742 Å is still not known (Koesterke et al. 1992, Hillier 1991). These two corrections do not affect the strength of the other lines considered here.

Slightly different models are applied in the second step when the analyses are refined by detailed line fits for each individual star. The corresponding calculations account for many more C IV levels, because now *all* C IV levels are split into angular momentum substates (s,p,d etc.) in order to avoid systematic errors especially concerning the determination of the carbon abundance (cf. Hamann et al. 1992). A further enlargement, accounting for C IV levels higher than $n = 10$, has no significant effect on the synthetic spectra (cf. Sect. 6). A summarizing description of the model atoms is given in Table 2.

Table 2. Model atom summary

	grid models		line-fit models	
Ion	non-LTE levels	lines	non-LTE levels	lines
He I	17	55	17	55
He II	16	120	16	120
He III	1	-	1	-
C II	3	2	3	2
C III	40	224	40	224
C IV	19	116	54	321
C V	1	-	1	-
total	97	517	132	722

3. The model grid

A grid of models for WC atmospheres with a carbon to helium ratio of 60:40 (by mass) has been established in a previous paper (Koesterke et al. 1992). Analogously we now present a grid with a smaller carbon mass fraction of $\beta_{\rm C} = 0.2$.

Contour plots of constant equivalent widths are shown for the five lines C III 5696 Å (Fig. 1), C IV 5470 Å (Fig. 2), He I 10830 Å (Fig. 3), He I 5876 Å (Fig. 4) and He II 5412 Å (Fig. 5). These lines are those strategic for the coarse analyses. Compared to the former grid with the higher carbon abundance ($\beta_{\rm C} = 0.6$) the contour shapes are very similar, but the absolute line strengths differ considerably. Carbon lines are generally affected more than helium lines. We close this section by displaying the contours of constant absolute visual magnitude $M_v^{\rm t}$ (Fig. 6) and contours of constant intrinsic color index $(b-v)_0$ (Fig. 7), always referring to the narrow-band colors as defined

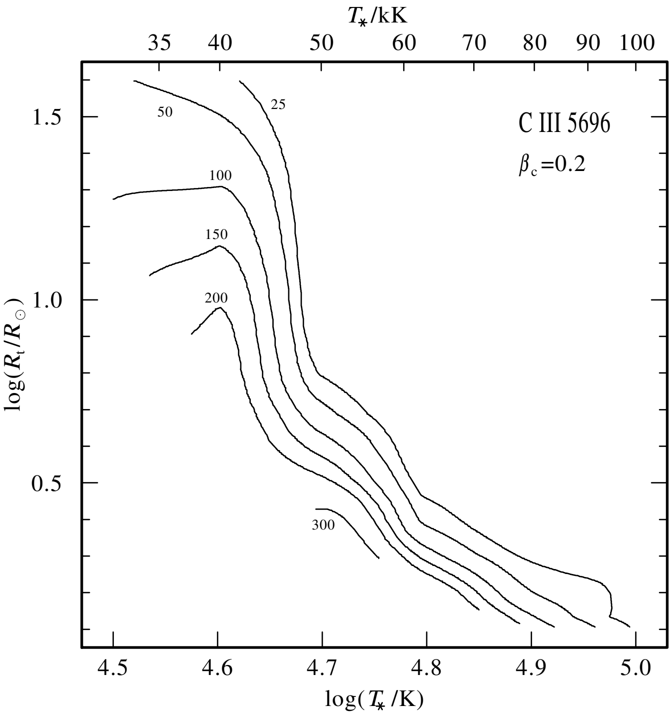

Fig. 1. Contours of constant equivalent width of C III 5696 Å. The labels denote $-W_\lambda$ in Å (emission). The only component is C III $3d\,^1D - 3p\,^1P^o$.

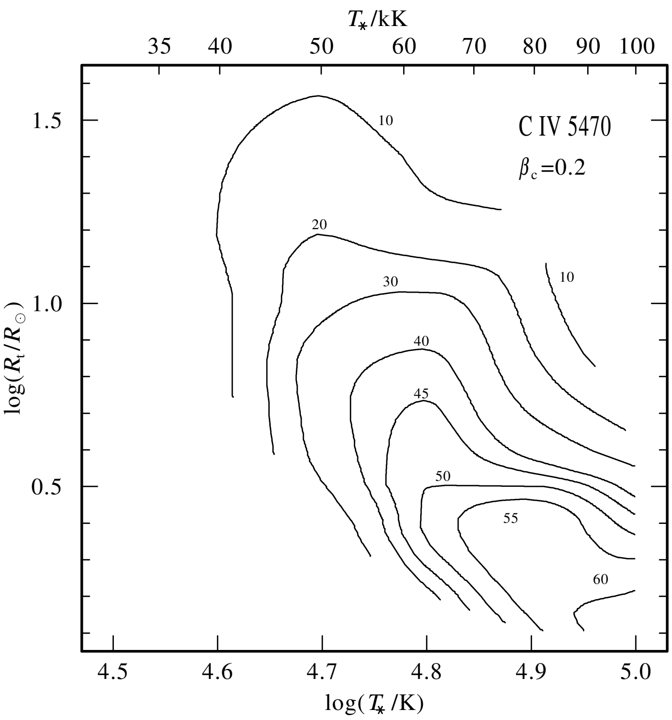

Fig. 2. Contours of constant equivalent width of C IV 5470 Å. The main component is C IV $10 - 7$.

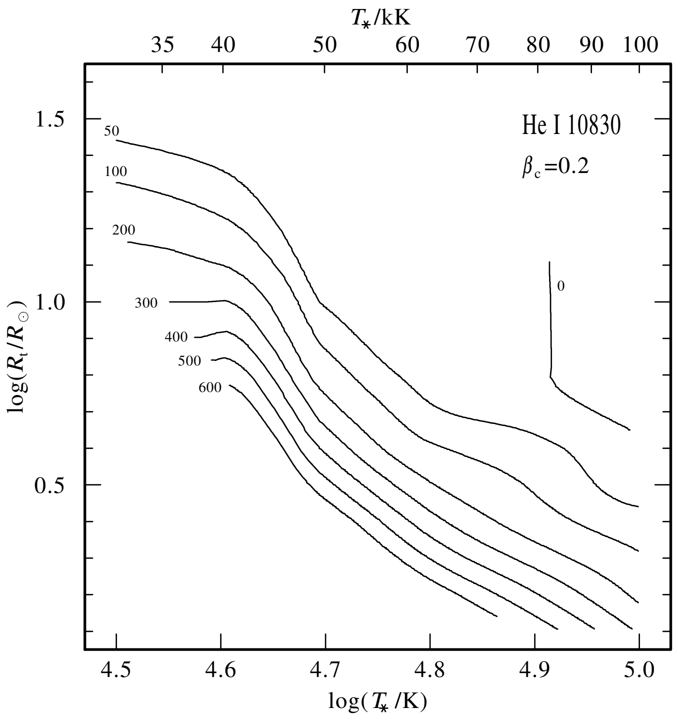

Fig. 3. Contours of constant equivalent width of He I 10830 Å. The main component is He I $2p\,^3P^o - 2s\,^3S$.

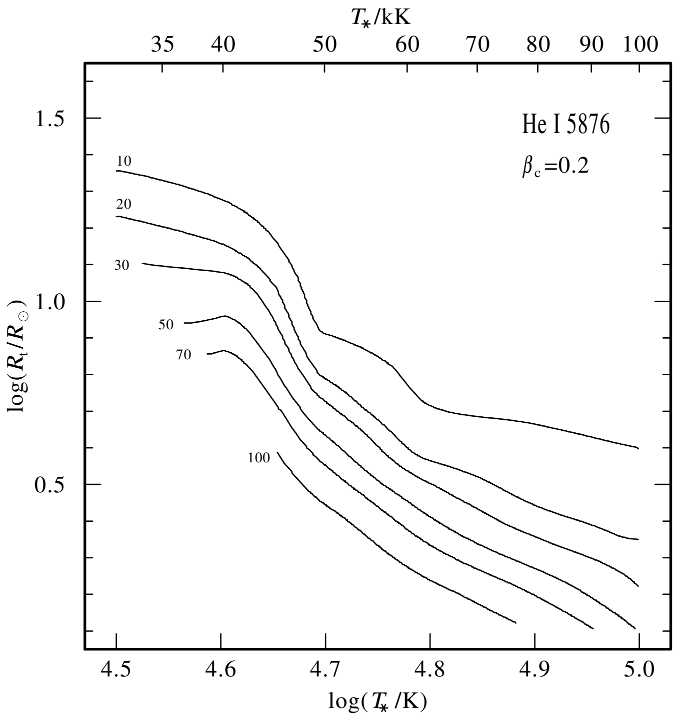

Fig. 4. Contours of constant equivalent width of He I 5876 Å. The main component is He I $2p\,^3P^o - 3d\,^3D$.

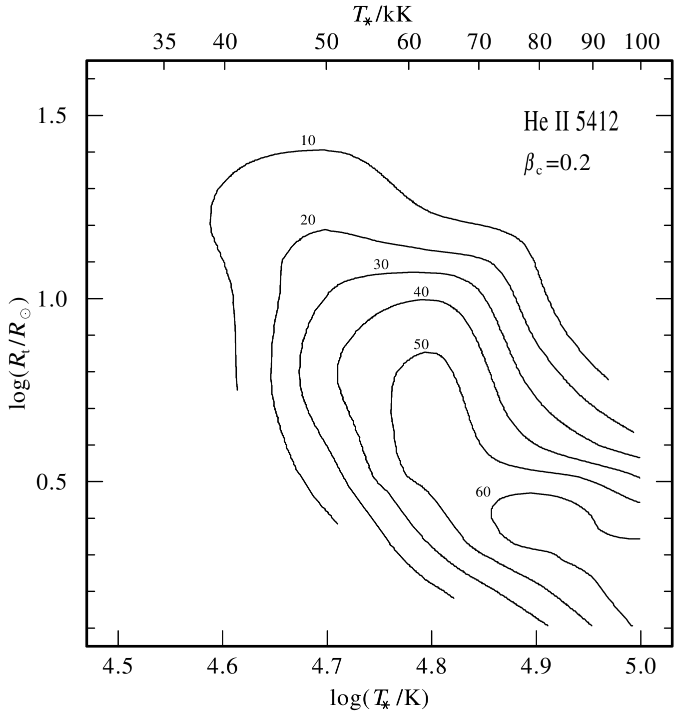

Fig. 5. Contours of constant equivalent width of He II 5412 Å. The main component is He II 7 − 4.

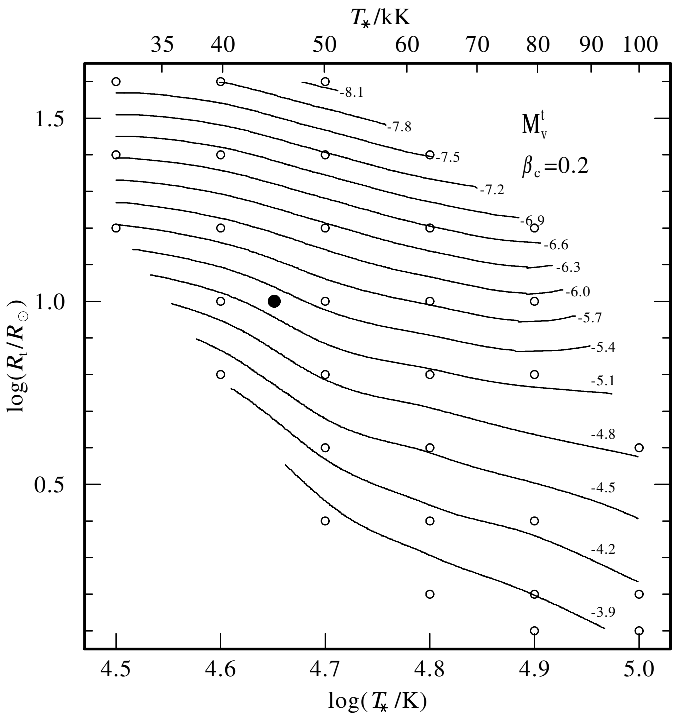

Fig. 6. Contours of constant absolute visual magnitude M_v^t (labels). The open circles denote the models of the grid. In anticipation of the following example analysis the position of WR 86 (filled circle) is indicated.

by Smith (1968). Note that the absolute visual magnitudes M_v^t of models with β_C = 0.2 do not differ significantly from those with β_C = 0.6. The positions of the 31 grid models are indicated in Fig. 6.

4. Observational data

We use the atlas of optical spectrophotometry of WC stars by Torres & Massey (1987), which provides a homogeneous set of optical spectrophotometric observations (3300-7300 Å). To match their moderate resolution, all synthetic spectra are convolved with a Gaussian of 8 Å FWHM. The classification is taken from van der Hucht et al. (1988) which is based on the classification of van der Hucht et al. (1981) with the revisions suggested by Torres et al. (1986).

In this work we only consider single stars. WR 86 is known as a visual binary seperated by about 2". However, since the companion is 1.5 mag fainter than the WC star (van der Hucht et al. 1988) and the aperture of the spectrograph was as small as 2", the contamination of the observed spectrum should be small. For WR 50 van Genderen et al. (1991) found intrinsic variations, but we feel that the evidence of a companion is not conclusive so far.

The spectra of WC stars are dominated by many strong and broad emission lines. In the optical range the continuum is visible only at a few wavelengths. Therefore the rectification of WC spectra is difficult, and often uncertain, especially when only short wavelength ranges have been observed. Some measured

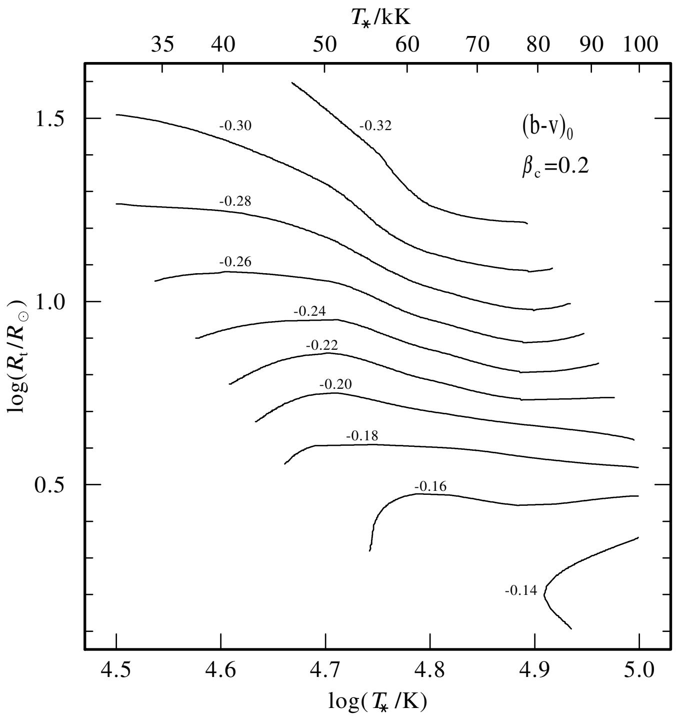

Fig. 7. Contours of constant intrinsic color index $(b-v)_0$.

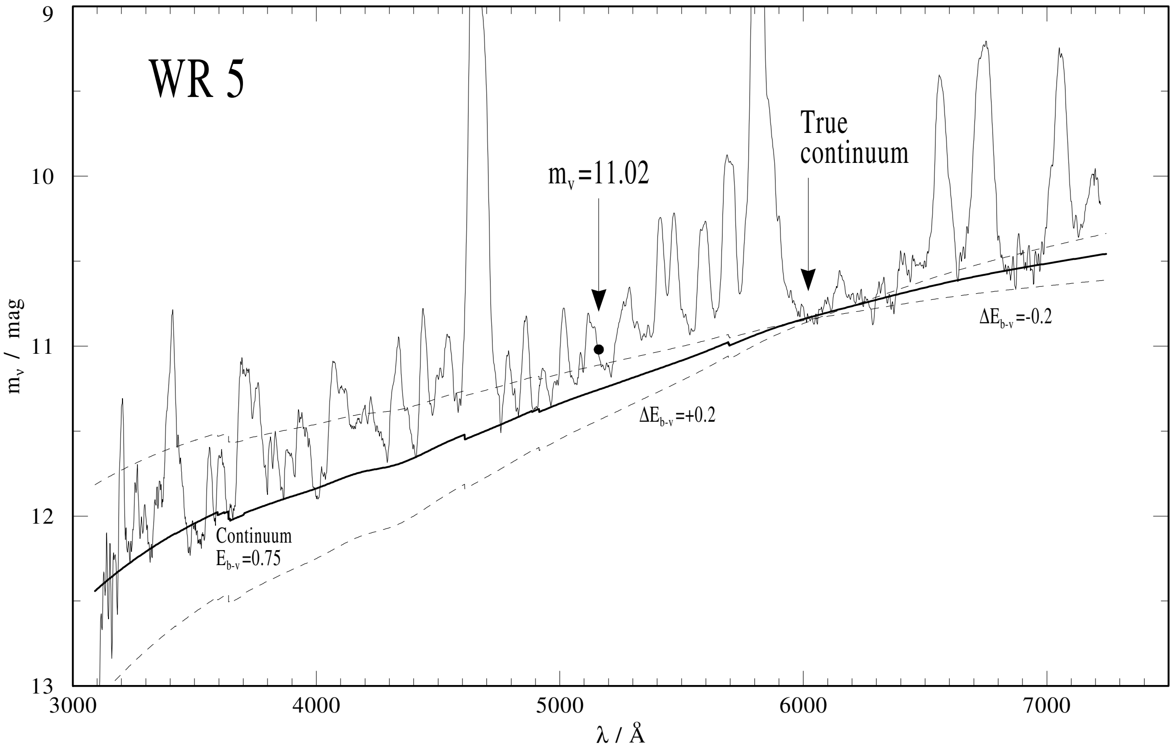

Fig. 8. Observation and theoretical model continuum for WR 5. The theoretical continuum of a grid model is displayed for three different reddening parameters E_{b-v}, always normalized at 6050 Å where we assume that the stellar continuum can be seen. The slope of the observed spectrum is well reproduced by the model continuum reddened with E_{b-v} = 0.75 (solid line). The two other continua (dashed lines, reddened with 0.2 mag more or less) differ considerably. Note that the narrow-band color m_v is considerably contaminated by line emission.

equivalent widths may differ by a factor of two, depending on the choice of the continuum.

In this work we reduce these uncertainties by rectifying the optical spectrophotometric observations of Torres & Massey (1987) with the theoretical fluxes of our models. We compare the observed flux distribution with the theoretical continuum flux, scaled to the observed apparent magnitude m_v and reddened with E_{b-v} as given by van der Hucht et al. (1988). If necessary we then adjust the color excess E_{b-v} suitably (final values are given in Table 3). Simultaneously the continuum is rescaled in the way that it fits the observation at the few wavelengths where the true stellar continuum is visible. This is illustrated in Fig. 8.

Note that the purpose of this procedure is the reliable rectification of the observed spectra, but not an accurate determination of the color excess. The latter would require to consider also the UV spectra. Moreover, we used the emergent flux of a "typical" model for the rectification, without any iteration with the final models for the individual stars. This can already induce errors in E_{b-v} up to 0.2 mag.

Finally the spectrum is divided by this theoretical continuum and the equivalent widths of several helium and carbon lines are measured (Table 3). The equivalent widths of He I 10830 Å listed in Table 4 originate from Kuhi (1968), Schmutz et al. (1989), Vreux et al. (1990) and Howarth & Schmutz (1992).

The absolute visual magnitudes M_v included in Table 3 are taken from van der Hucht et al. (1988). Seven stars of our sample are known to be open cluster or association members (cf. Table 5), and in these cases the absolute brightness follows from the apparent brightness, the distance and the interstellar extinction. The latter can be estimated from the color excess. The values for E_{b-v} used by van der Hucht et al. (1988) for that purpose are confirmed by our continuum fits (see above) within relevant accuracy.

Based on the WC stars with known distances (i.e. open cluster and association members), van der Hucht et al. (1988) calibrated M_v versus subtype (WC 5 and WC 6: M_v=-3.7 mag; WC 7 and WC 8: M_v=-4.8 mag). This calibration must be considered as very uncertain, because i) the fraction of WC stars with known distances is small; for subtype WC 7 there even exists no representative single-star (only binaries); ii) the correlation of M_v with subtype shows a large scatter; iii) binaries are included in the calibration sample although they might behave differently.

5. The coarse analyses

The coarse analyses are based on the comparison of measured equivalent widths with the contour diagrams of the model grid. This technique, which has been employed to all 25 program stars, is comprehensively explained in Koesterke et al. (1992).

Table 3. Visual magnitudes (van der Hucht et al. 1988), color excesses, and emission line equivalent widths (in Å)

Name	Type[(1)]	m_v	M_v	E_{b-v}	C III 5696	C IV 4441	C IV 5017	C IV 5470	He I 5876	He II 4860	He II 5412	5412+ 5470	Comment
WR 4	WC 5-s	10.53	-3.7	0.47	121	48	31	63	-	22	43	106	
WR 17	WC 5-s	11.11	-3.7	0.31	68	42	27	49	-	39	60	109	
WR 33	WC 5-s	12.34	-3.7	0.47	162	≈93	≈39	≈81	-	-	≈35	116	blend of 5412 & 5470
WR 52	WC 5-s	9.98	-3.7	0.42	107	56	48	75	-	33	49	124	
WR 111	WC 5-s	8.23	-3.8	0.25	102	54	33	55	-	29	35	90	
WR 114	WC 5-s	12.95	-3.6	1.18	101	39	22	46	-	20	42	88	
WR 126	WC 5-w	13.29	-3.7	0.85	<19	-	-	≈11	-	-	≈30	41	weak lines
WR 143	WC 5-w	11.95	-3.7	1.48	<33	≈25	-	≈36	-	-	≈26	62	blend of 5412 & 5470
WR 150	WC 5-s	13.47	-3.7	0.80	≈106	47	34	≈69	-	24	≈55	124	blend of 5412 & 5470
WR 5	WC 6-s	11.02	-3.7	0.75	100	39	21	48	-	21	48	96	
WR 13	WC 6-s	13.83	-3.7	1.14	112	39	25	56	-	22	47	113	
WR 14	WC 6-s	9.42	-3.8	0.42	223	46	18	52	-	19	46	98	
WR 15	WC 6-s	11.73	-3.7	1.16	176	36	20	≈45	-	24	≈59	104	blend of 5412 & 5470
WR 23	WC 6-s	9.71	-3.7	0.31	237	67	24	64	-	20	47	111	
WR 27	WC 6-s	14.73	-3.7	1.41	156	51	46	54	-	24	43	97	
WR 39	WC 6-w	14.10	-3.7	1.49	63	-	-	≈14	-	-	≈15	29	blend of 5412 & 5470
WR 50	WC 6-w	12.49	-3.6	0.91	162	-	-	≈26	-	-	≈26	52	blend of 5412 & 5470
WR 132	WC 6-s	13.49	-3.7	0.97	205	47	33	58	-	21	42	100	
WR 154	WC 6-s	11.54	-3.7	0.63	160	41	31	56	-	24	45	101	
WR 56	WC 7-s	13.97	-4.8	0.80	249	81	39	46	≈29	32	32	78	
WR 57	WC 7-s	10.11	-4.8	0.25	436	78	46	52	≈68	30	34	86	
WR 68	WC 7-s	14.23	-4.8	1.36	213	45	17	39	≈89	24	51	90	
WR 86[(2)]	WC 7-w	9.73	-4.8	0.75	114	23	13	21	≈23	6	16	37	4860 near detection
WR 125	WC 7-w	13.52	-4.8	1.49	198	-	-	≈29	-	-	≈31	60	blend of 5412 & 5470
WR 135	WC 8	8.36	-4.7	0.35	294	36	21	28	73	24	33	61	

(1) Among the WC 5 to WC 7 stars we distinguish two groups, depending on whether the sum of the equivalent widths of He II 5412 Å and C IV 5470 Å is weaker (WC-w) or stronger (WC-s) than 70 Å (see text).
(2) Visual binary

Table 4. Emission line equivalent widths of He I 10830 Å (in Å) from different sources

Type	Name	(1)	(2)	(3)	(4)
WC 5	WR 4	154	-	153	
	WR 111	115	180	177	90
	WR 114	195	-	-	-
	WR 143	61	-	(32)	-
WC 6	WR 5	225	-	213	
	WR 14	-	300	-	-
	WR 23	-	260	-	-
	WR 132	97	-	161	-
	WR 154	211	-	226	220
WC 7	WR 86[(5)]	-	120	-	-
WC 8	WR 135	295	-	321	-

(1) Kuhi (1968)
(2) Schmutz et al. (1989)
(3) Vreux et al. (1990)
(4) Howarth & Schmutz (1992)
(5) Visual binary

From the contour diagrams of the model grid (cf. Figs. 1-5) we extract those contours corresponding to the observed equivalent widths (cf. Tables 3 and 4) and superimpose them into one diagram. This is done twice for both grids with the different carbon abundances as exemplarily shown for WR 86 in Fig. 9. In both diagrams a carbon "fit point" (filled triangle) is determined as the point of intersection of C III 5696 Å and C IV 5470 Å. A helium "fit point" (filled square) is determined using He I 5876 Å, He I 10830 Å and He II 5412 Å. The fit lines for He I 5876 Å and He I 10830 Å do not differ significantly in cases when data for both lines are available. Note that we have used the C III 5696 Å line as a replacement of the He I lines for those stars for which no He I 10830 Å equivalent width is available and the He I line at 5876 Å is strongly blended with the C IV 5805 Å doublet. In each of the diagrams a compromise "fit point" (filled circle) is assumed to lie in the middle of the corresponding carbon and helium "fit points".

In a next step the carbon abundance is estimated from the discrepancy between the helium and the carbon "fit points" (cf. Fig. 9). If the carbon abundance matches the grid value, all contours should intersect at one "fit point" in the ideal case. The example shows that the helium and carbon "fit points"

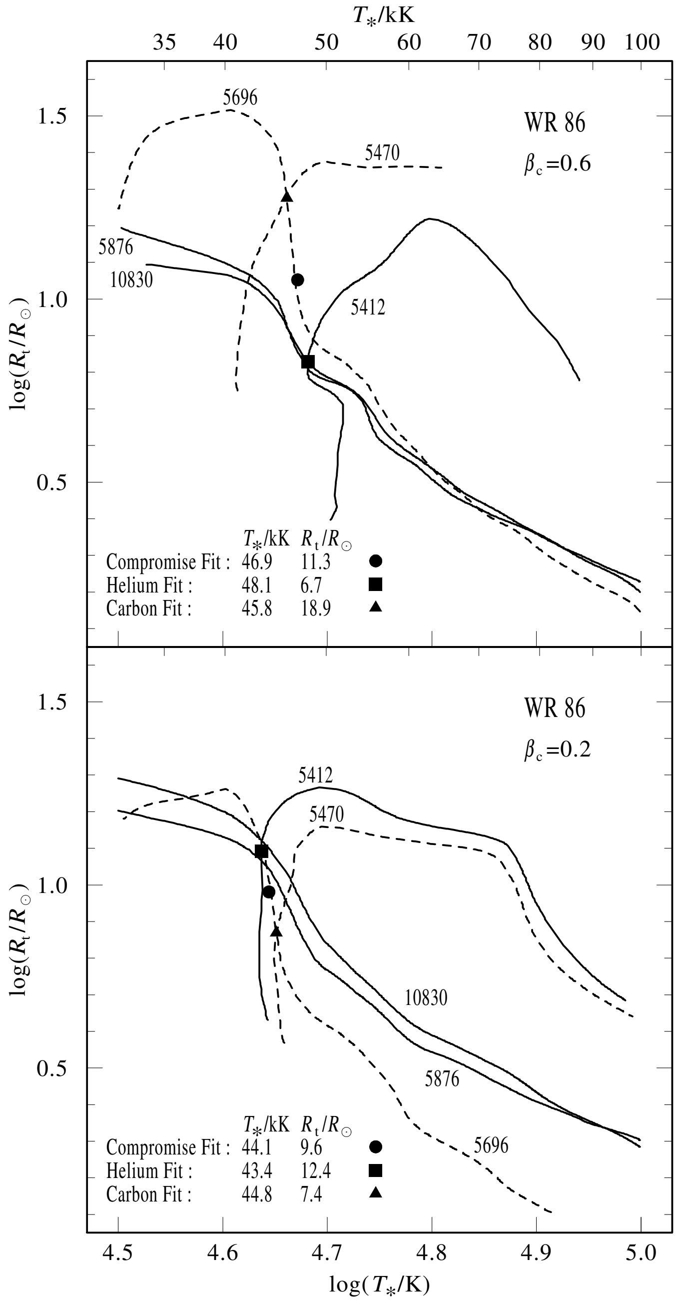

Fig. 9. Example of a coarse analysis (WR 86). Those contours corresponding to the observed equivalent widths are extracted from the model grids (β_C=0.6: upper panel; β_C=0.2: lower panel). In both panels the points of intersection of the carbon lines (C III 5696 Å and C IV 5470 Å) and the helium lines (He I 10830 Å, He I 5876 Å and He II 5412 Å) are determined. The actual carbon abundance and the final stellar parameters are estimated from the discrepancy between these "fit points" by linear interpolation (see text). In this particular example we obtain β_C = 0.3, T_* = 44.8 kK and R_t = 10.0 $R_\odot$.

interchange their relative positions comparing the β_C = 0.2 and the β_C = 0.6 diagram. This indicates that the actual carbon abundance is between these values. Assuming a linear relation, the carbon abundance and the final parameters are obtained by interpolation.

We proceed with the technique described by Koesterke et al. (1992) to determine the stellar radius R_* and the mass-loss rate $\dot{M}$. For that purpose the absolute visual magnitude M_v^t which corresponds to the final temperature T_* and the transformed radius R_t of the stars are read off the model grid (cf. Fig. 6). Then the stellar radius R_* is determined from the difference between the visual magnitude M_v and M_v^t by

$$\left(\frac{R_t}{R_*}\right)^2 = 10^{0.4(M_v - M_v^t)} . \qquad (2)$$

Finally, after estimating the terminal velocities v_∞ from the maximum widths of the C III line at 5696 Å, the mass-loss rate $\dot{M}$ is given by

$$\log\left(\frac{\dot{M}}{M_\odot\, yr^{-1}}\right) = 0.3\,(M_v^t - M_v) + \log\left(\frac{v_\infty}{2500\,\mathrm{km\,s^{-1}}}\right) - 4.0 . \qquad (3)$$

6. Test calculations

Before proceeding to the "fine analyses" we have tested three modifications of the model atom, the influence of the velocity law exponent, of the microturbulence parameter, and of the frequency redistribution of line photons by electron scattering. These tests are described in the following.

While in the model grid calculation the C IV levels with principal quantum numbers $n \geq 5$ are not split into angular momentum substates, we now account for the different substates explicitely. The effect on the He II/C IV blend at 5412/5470 Å is demonstrated in Fig. 10. The use of the smaller C IV model atom leads to an underestimate of the carbon abundance by about 0.1 (mass fraction). Because of this large effect we carried out the fine analyses with the split C IV levels.

In a second test we accounted for additional C IV levels with principal quantum numbers n = 11 up to n = 20 and encountered remarkably small effects on the line strength. This is illustrated in Fig. 11. Because of the high computational cost, especially the large increase of the number of line transitions, and the small effect on the line strengths, compared to the first test, we neglect these high C IV levels in the models for the fine analyses.

In a third test we investigate the effect of an detailed C II model atom on the synthetic spectra. The test was performed with the parameters of the latest subtype in our sample, the WC 8 stars WR 135. In our standard calculations only three C II states are accounted for. The detailed C II model atom (32 levels, 147 lines) was developed by Leuenhagen & Hamann (1994). The indirect effect on the He, C III and C IV lines turned out to be almost invisible. The only C II feature in the visible

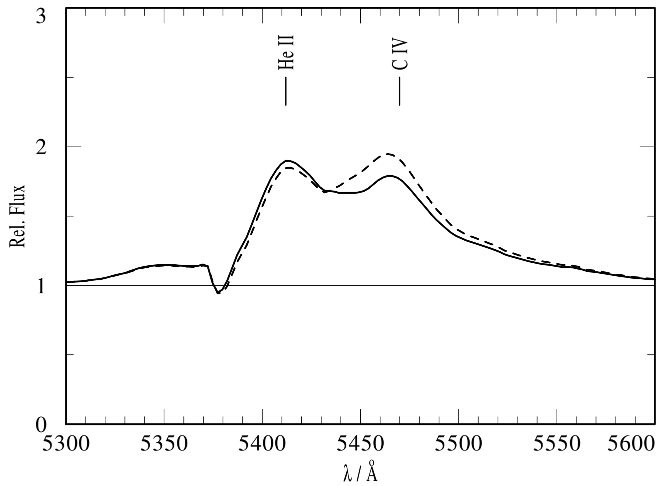

Fig. 10. Test calculations with an improved C IV model atom (dashed profile). The solid profile is calculated with the same model parameters, but the simpler model atom used for the model grid, in which C IV levels with principal quantum numbers $n \geq 5$ are not split into angular momentum substates. The use of the smaller C IV model atom would lead to an underestimate of the carbon abundance by about 0.1 (mass fraction). The synthetic profiles are calculated with the final parameters for WR 114 (cf. Table 5) and convolved with a Gaussian of 8 Å FWHM.

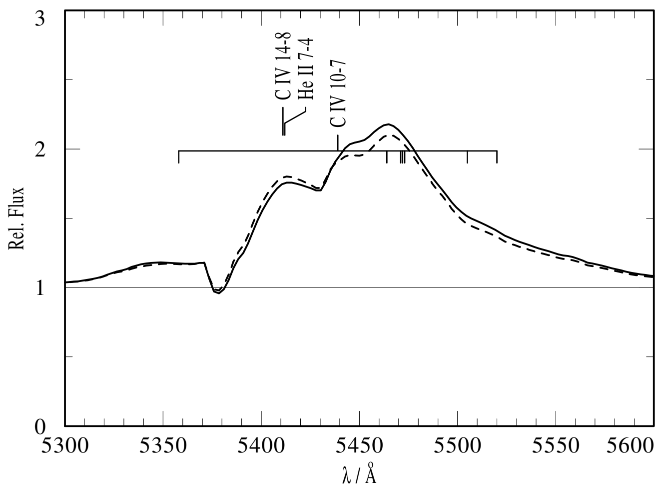

Fig. 11. Testcalculations with an improved C IV model atom. The dashed profile is calculated with the same model parameters but including C IV levels with principal quantum numbers $11 \leq n \leq 20$ while the solid profile is calculated with the simpler model atom used for the grid. For illustration the He II and C IV components are indicated. In both calculations all C IV levels with $n > 5$ are not split into angular momentum substates, but in the formal solution the substates of C IV $n = 7$ and $n = 10$ are accounted for. The He II line at 5412 Å is hardly affected by its carbon counterpart (14-8). The change of C IV 5470 Å does mainly result from the fact, that the upper level of the transition is the highest C IV level in the smaller C IV model atom. The synthetic profiles are calculated with the final parameters for WR 111 (cf. Table 5) and convolved with a Gaussian of 8 Å FWHM.

spectrum, namely the small contribution of C II 6580 Å to the helium line at 6560 Å, is shown in Fig. 12.

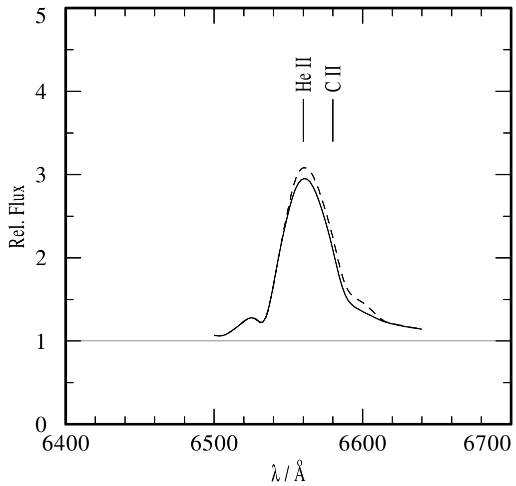

Fig. 12. Effect of a detailed C II model ion (dashed profile) on the He II 6560/C II 6580 Å line blend. The solid profile is calculated with the simpler C II model ion with only three levels as used for the model grids. Both synthetic profiles are calculated with the final parameters of WR 135 (cf. Table 5) and convolved with a Gaussian of 8 Å FWHM.

Test calculations with different microturbulence and different velocity-law exponents are motivated by problems in fitting the profile shape of the He II 5412 Å/C IV 5470 Å blend. In some spectra the depression between these two lines is deeper than reproduced by the models, in others that depression is weaker than calculated. Test calculations with various choices of v_D and β reveal that the depression can be weakened with a small velocity-law exponent of $\beta \approx 0.4$ (cf. Fig. 13). Spectra which show a strong depression between both features cannot be reproduced by models with different v_D or by models with different β.

Finally we study the influence of the frequency redistribution of line photons by electron scattering on the He II and C IV lines at 5412 Å and 5470 Å, respectively. The importance of this effect, which we account for in the Formal Integral (cf. Hamann et al. 1992), is demonstrated in Fig. 14 by means of the He II/C IV blend at 5412/5470 Å, showing the final models for WR 114 and WR 150 (see Table 5 for the parameters). The He II and the C IV blend components become stronger, but the effect on the C IV lines is pronounced. Hence the inclusion of this effect has some influence on the derived carbon abundance.

7. Fine analyses

Due to three reasons the results of the coarse analyses technique applied to WC stars are less reliable than in the case of pure-helium analyses of WN spectra.

- Most important, one more stellar parameter, the carbon content of the atmosphere, has to be determined by interpolation between two model grids.

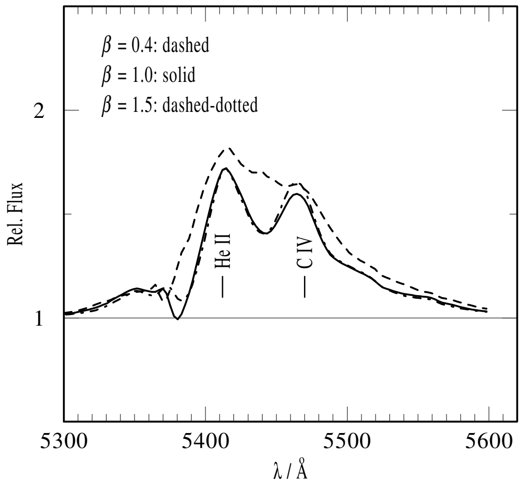

Fig. 13. Synthetic profiles of the He II 5412 Å and C IV 5470 Å line blend for different exponents of the velocity law (parameters as for WR 125, cf. Table 5). The synthetic profiles of three models with β = 0.4 (dashed), β = 1.0 (solid) and β = 1.5 (dash-dotted) are displayed. The depression in the middle is removed by choosing a small β. Both other models show the lines more separated. The synthetic profiles are convolved with a Gaussian of 8 Å FWHM.

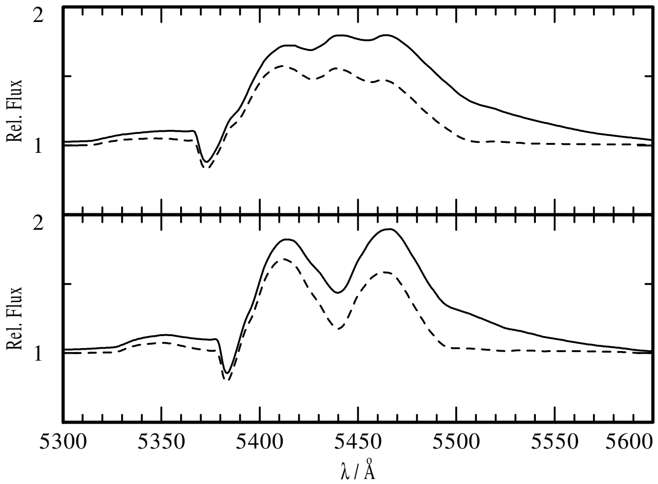

Fig. 14. The effect of frequency redistribution of line photons by electron scattering (solid line) on the He II5412 Å/C IV5470 Å blend. The dashed profiles are calculated with the mean intensity of the continuum (J_C). The examples are calculated with the final parameters (cf. Table 5) for WR 150 (upper panel) and WR 114 (lower panel), respectively

- The spectra of WC stars contain many more broad emission lines forming complex blends. Therefore the equivalent widths of individual lines can often not be measured accurately.
- The crowding of emission lines prevents an accurate determination of the continuum. Although we have overcome this problem by our procedure of rectification with a model continuum, the equivalent widths remain uncertain by up to 25%.

After we have performed the coarse analyses we have calculated individual models for the stars taking the stellar parameters of the coarse analyses. The comparision of the synthetic profiles with the observations turned out to be unsatisfactory. Therefore we have performed a series of models for each of the program stars, adjusting the model parameters such that the synthetic lines profiles give an optimum fit to the observation. For these fine analyses we use all spectral lines but attaching special impotance to those which we call strategic (ct. Sect. 3).

The quality of the coarse analyses turned out to be poor. For almost all stars the stellar temperature T_* is underestimated. About one third of the stars show discrepancies of more than 15 kK up to 30 kK in temperature and of 0.2 to 0.3 in the carbon mass fraction between the results of the coarse and the fine analyses. This is examplarily discussed for WR 5 which fit quality is rated good (cf. Table 5). From the coarse analysis we have estimated T_* = 59 kK, R_t = 2.9 $R_\odot$ and β_C = 0.2 which is clearly different from the results of the fine analysis (T_* = 93.3 kK, R_t = 1.6 $R_\odot$, β_C = 0.4). In the first individual model for WR 5, calculated with the parameters of the coarse analysis, the peak height of He II 5412 Å and C IV 5470 Å was underestimated by a factor of 1.5. This discrepancy was resolved by clearly hotter models with higher wind densities (smaller R_t). Since the He II and C IV lines behave different, a large change of the carbon content was also necessary. From these experiences we dissuade readers from applying the model grids without reviewing the results using at least one individual model.

The parameters obtained from these "fine analyses" are listed in Table 5. In the last column the quality of the achieved fit is rated. To this almost all carbon and helium lines are considered. Also the following three criteria are used.

a: Discrepancies between the two C III lines at 5696 Å and 6742 Å. Remember that the strength of C III 6742 Å suffers from uncertainties in the atomic data (cf. Sect 2).
b: Differences between the observed and the synthetic profile shapes of the He II 5412 Å/C IV 5470 Å blend as discussed in Sect. 7.
c: The reproduction of the peak heights of He II 5412 Å and C IV 5470 Å.

The fit quality of ten stars is very good (rating "++"). Almost all observed helium and carbon lines are well reproduced in both their absolute strength and the profile shape. The fit quality of nine stars is good ("+"). Discrepancies occurred concerning the profile shapes of He II 5412 Å and C IV 5470 Å as described by criterion **b**. Three stars (WR 56, 57, 68) show medium discrepancies between C III 5696 Å and C III 6742 Å (criterion **a**). For these 19 stars we estimate an error in the carbon abundance of 0.1. For six stars no satisfactory fit is achieved (rating "-"). The peak heights of He II 5412 Å and C IV 5470 Å are not reproduced (criterion **c**). Therefore the stellar temperature could not be determined with accuracy. Furthermore some analyses suffer from large discrepancies between the C III lines at 5696 Å and 6742 Å (criterion **a**).

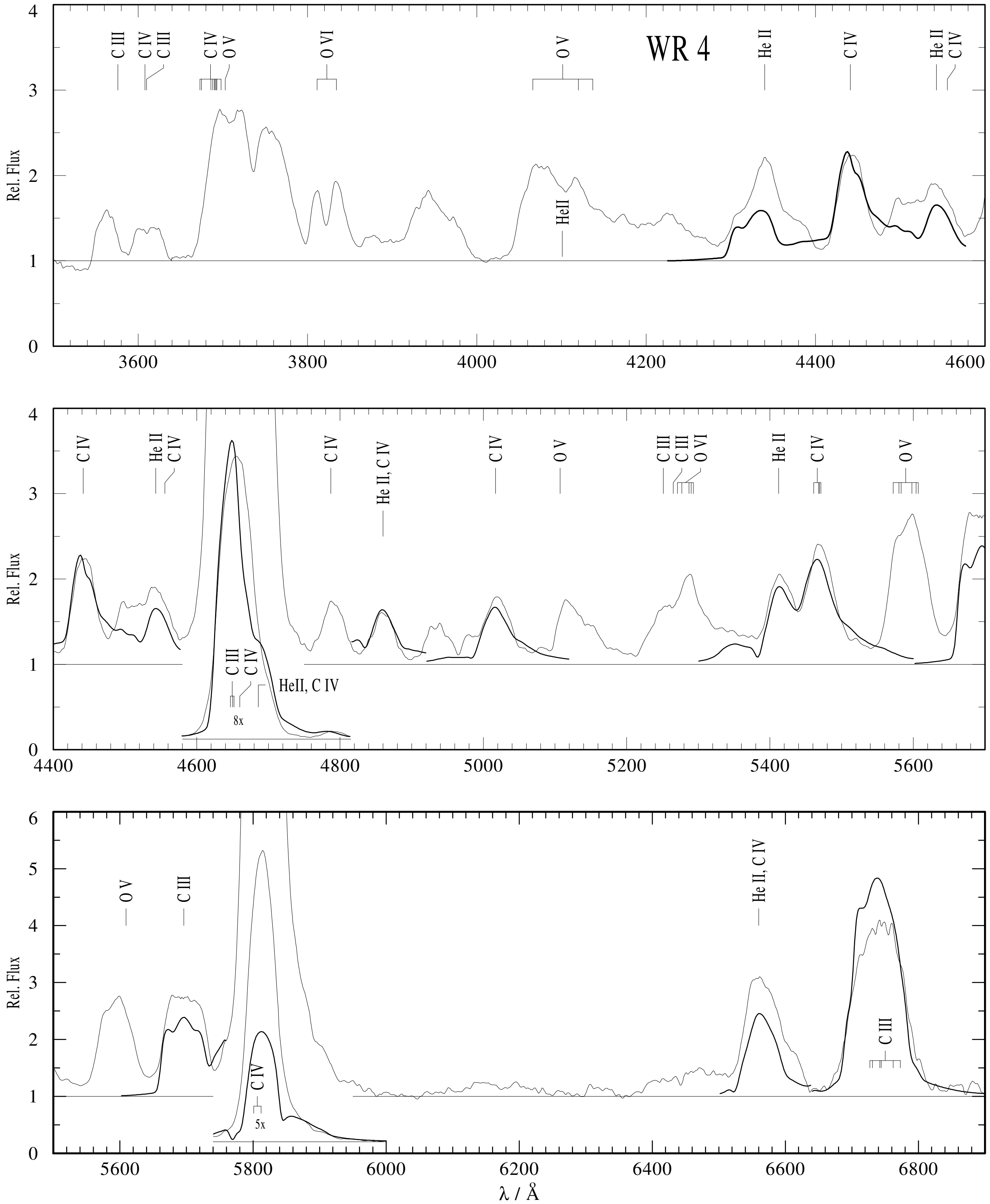

Fig. 15. Observed rectified spectrum of WR 4 (WC 5-s) and theoretical line profiles (thick lines). The important carbon, helium and oxygen lines are identified. Most carbon and helium features are well reproduced. All synthetic profiles are calculated with the final parameters for WR 4 (cf. Table 5) and convolved with a Gaussian of 8 Å FWHM.

Table 5. Results of the fine analyses. $T_{2/3}$ and $R_{2/3}$ refer to an Rosseland optical depth of $\tau = 2/3$ while T_* and R_* refer to $\tau \approx 20$. The carbon abundances are mass-fractions assuming a pure helium-carbon composition. Stars with a known distance are marked in the column entitled "d?".

Type	Name	T_* [kK]	$T_{2/3}$ [kK]	R_t [$R_\odot$]	R_* [$R_\odot$]	$R_{2/3}$ [R_*]	$\log \dot{M}$ [$M_\odot\,\mathrm{yr}^{-1}$]	v_∞ [$\mathrm{km\,s^{-1}}$]	β_C [mass fraction]	$\log L$ [$L_\odot$]	d?	Fit quality
WC 5-w	WR 126	59.3	56.8	12.	4.0	1.1	-4.8	2500	0.20	5.2		+(1)
	WR 143	50.7	47.3	10.	4.3	1.1	-4.5	3200	0.40	5.0		+
WC 5-s	WR 4	74.1	38.6	2.2	1.8	3.7	-4.2	1900	0.50	5.0		++(2)
	WR 17	97.7	39.8	1.4	1.2	6.0	-4.2	1800	0.30	5.1		–
	WR 33	66.4	39.0	2.8	2.2	2.9	-4.1	2900	0.50	4.9		++
	WR 52	78.5	38.6	2.0	1.7	4.1	-4.2	2200	0.55	5.0		++
	WR 111	62.5	40.6	3.6	2.7	2.4	-4.3	2000	0.50	5.0	x	++
	WR 114	63.1	35.0	2.5	2.0	3.3	-4.3	1900	0.40	4.7	x	++
	WR 150	70.8	37.5	2.3	1.9	3.6	-4.1	2600	0.40	4.9		++
WC 6-w	WR 39	49.0	48.5	18.	4.7	1.0	-4.7	3600	0.40	5.1		+
	WR 50	49.0	45.5	10.	5.0	1.2	-4.4	3000	0.50	5.1	x	+
WC 6-s	WR 5	93.3	41.2	1.6	1.4	5.1	-4.3	1600	0.40	5.1		++(2)
	WR 13	97.7	40.7	1.4	1.2	5.8	-4.3	1700	0.40	5.1		–
	WR 14	85.9	35.2	1.4	1.3	6.0	-4.2	1800	0.30	4.9	x	–(3)
	WR 15	75.7	35.0	1.9	1.7	4.7	-4.0	2700	0.30	4.9		++(2)
	WR 23	79.6	35.6	1.6	1.5	5.0	-4.1	2200	0.45	4.9	x	++(2)
	WR 27	97.7	42.0	1.5	1.3	5.4	-4.2	1850	0.45	5.1		–(3)
	WR 132	95.5	42.7	1.6	1.3	5.0	-4.2	2000	0.50	5.1		–(3)
	WR 154	70.8	36.0	2.2	1.9	3.9	-4.2	2050	0.40	4.9	x	++(2)
WC 7-w	WR 86(4)	47.8	46.0	14.	8.0	1.1	-4.4	2300	0.60	5.5		+
	WR 125	48.0	25.8	6.5	6.0	3.5	-4.0	2800	0.30	5.2		+
WC 7-s	WR 56	60.3	32.3	2.8	3.9	3.5	-3.9	1800	0.50	5.3		+
	WR 57	85.6	35.5	1.7	2.5	5.8	-4.0	1500	0.50	5.5		+
	WR 68	95.5	36.1	1.4	2.0	7.0	-3.9	2050	0.20	5.5		+
WC 8	WR 135	75.9	33.3	1.9	2.6	5.2	-4.1	1300	0.30	5.3	x	–(3)

(1) Very weak C III lines
(2) Small discrepancies between the C III lines at 5696 Å and 6742 Å
(3) Large discrepancies between the C III lines at 5696 Å and 6742 Å
(4) Visual binary

In Fig. 15 the observed spectrum of WR 4 is shown together with the synthetic profiles of the final model as an example for a fit of good quality.

8. Results and Discussion

In this section the results of the fine analyses are discussed. In the Sects. 8.1 to 8.3 we investigate the distance-independent quantities T_*, R_t, β_C, v_∞ and the spectral subtype. After that we comment on the luminosities of the WC stars with regard to the absolute scaling (Sect. 8.4). Then we show the WC and WN stars together in one HRD (Sect. 8.5). Finally the properties of the WR stars are compared with predictions from theoretical tracks and conclusions on the evolutionary status are drawn (Sect. 8.6).

8.1. The WC stars in the T_*-R_t-plane

Figure 16 shows the positions of the analyzed WC stars in the T_*-R_t-plane. Note that these two parameters follow from the spectral analysis alone and do not involve the assumed distance or absolute magnitude. In that diagram the stars arrange themselves into two distinct groups which can be characterized by a simple spectroscopic criterion, namely whether the sum of the equivalent widths of He II 5412 Å and C IV 5470 Å is stronger than 70 Å (WC-s) or weaker (WC-w). This holds for the WC 5 to WC 7 subtypes; the only WC 8 in our sample obviously belongs to the WC-s group, although the equivalent widths sum is only 61 Å.

WC-w: These stars have large transformed radii (low wind density) and relatively low stellar temperatures ($T_* \approx 50$ kK) with increasing temperatures towards earlier subtypes. Although WR 126 has a considerably higher temperature than the other WC 5 star (WR 143), it can be assigned to this group. Its high temperature follows from the weakness of the C III lines in the observed spectrum. Most of the WC-w stars have non-extended atmospheres (except WR 125), which means that the continua arise from almost hydrostatic layers, i.e. $R_{2/3} \approx R_*$. The profile shapes of all these stars indicate that the velocity law exponent is as small as $\beta \approx 0.4$ rather than unity.

WC-s: These stars form a narrow strip in the T_*-R_t-plane extending from T_* = 60 kK and R_t = 3.1 $R_\odot$ to T_* = 100 kK and R_t = 1.2 $R_\odot$. The WC 5 stars, which show the highest-ionized spectra, lie at the upper edge of that strip. The later subtypes are arranged below them. All stars of this group have extended atmospheres, i.e. the continuum-forming layers have already reached high expansion velocities ($R_{2/3} \gg R_*$). The profile shapes of most stars are well reproduced by models with β = 1.

The introduction of a WC-s and WC-w classification is in parallel to a similar definition for early-subtype WN stars (WNE, i.e. up to WN 6). Following Schmutz et al. (1989), WNE stars are characterized as WNE-w or WNE-s depending on whether the equivalent width of He II 5412 Å is smaller or larger than 40 Å, respectively. As in the case of WC-s stars, the WNE-s group has "extended" atmospheres, while the WNE-w and WNL atmospheres are not "extended" using the terminology introduced above. In the T_*-R_t-plane the WC stars (Fig. 16) form a similar pattern as the WN stars (cf. Hamann et al. 1993, 1994). The WNE-w and WC-w groups both have almost constant temperatures ($\approx$ 35 kK for the WNE-w compared with $\approx$ 50 kK for the WC-w), while the WNE-s stars populate a similar strip extending to higher temperatures as the WC-s stars.

8.2. Subtype and terminal velocity

The terminal wind velocities are plotted versus the spectral subtype in Fig. 17. Some loose correlation exists for the subgroup of stars with strong lines (filled symbols), as indicated by the shaded strip. Stars with weak lines (open symbols) have generally higher terminal wind velocities which are not obviously correlated with their subtype.

8.3. The carbon abundance

Very important for the understanding of the evolution of WC stars is the chemical surface composition. Previous analyses were not based on detailed model atmospheres, but on recombination theory. Eenens & Williams (1992) and Smith & Hummer (1988) investigated the carbon content of six and 17 WC stars, respectively. Both groups found a correlation in the way of decreasing carbon content towards "later" spectral subtype. The results of Smith & Hummer (1988) were used for comparison with the standard evolutionary tracks (Smith & Maeder 1991) and considered as an empirical confirmation. On the contrary, Torres (1988) who investigated the largest sample (74 WC stars) found no clear correlation but a large scatter of the carbon content among each subclass.

The carbon abundances obtained from our detailed analyses are plotted versus spectral subtype in Fig. 18. No clear correlation can be seen thus confirming the results of Torres (1988), at least as far as only the intermediate subtype WC 5-7 are concerned. There is also no correlation between the carbon abundance and stellar parameters like T_*, $T_{2/3}$, R_t and L.

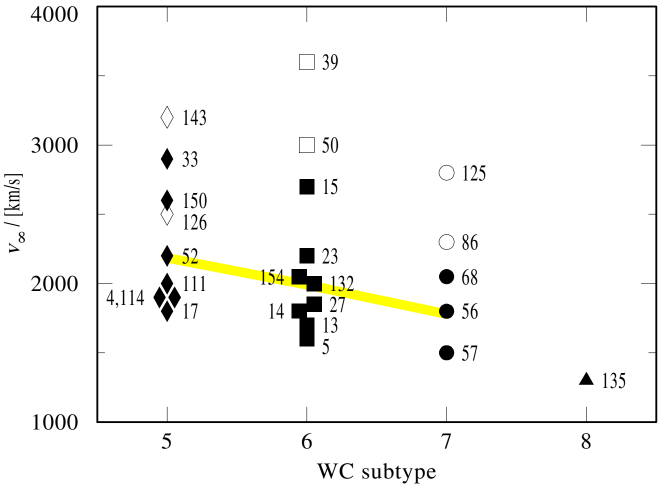

Fig. 17. The terminal velocity versus spectral subtype. The stars with strong lines (WC-s, filled symbols) show a correlation of decreasing terminal velocity for stars of later subtypes. The average values for the stars of this group are connected by the shaded line. For the stars with weak lines (WC-w, open symbols) the terminal velocities are clearly higher but not correlated with the subtype.

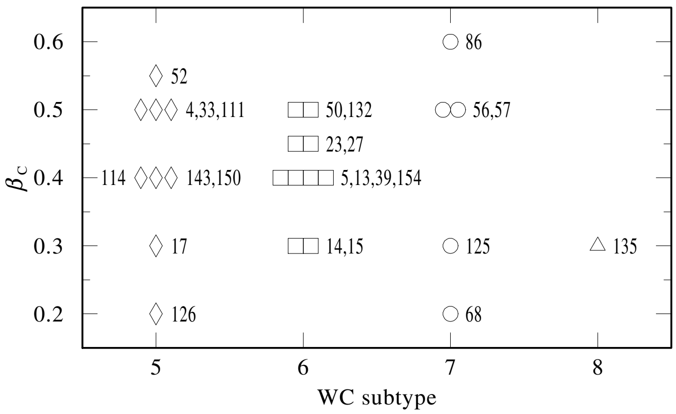

Fig. 18. Carbon mass fraction versus subtype classification. There is no clear correlation but a large scatter among the stars of the subclasses WC 5 to WC 7.

8.4. Luminosities

The determination of the luminosities (as well as the radii and the mass-loss rates) requires the knowledge of one distance-dependent quantity, e.g. the absolute magnitude M_v (cf. Sect. 5). As discussed in Sect. 4, for most stars (except the cluster/association members), M_v comes from the subtype calibration which is very uncertain. For the Galactic WN stars, Hamann et al. (1993) could improve the M_v calibration by considering not only the subtypes but also T_* and R_t. For the WC stars we could not establish a similar calibration from the seven stars with known distance in our sample mainly because of their small number. Thus the absolute parameters (L, $\dot{M}$, R_*) given in Table 5 are only definite for those stars marked in the column "d?".

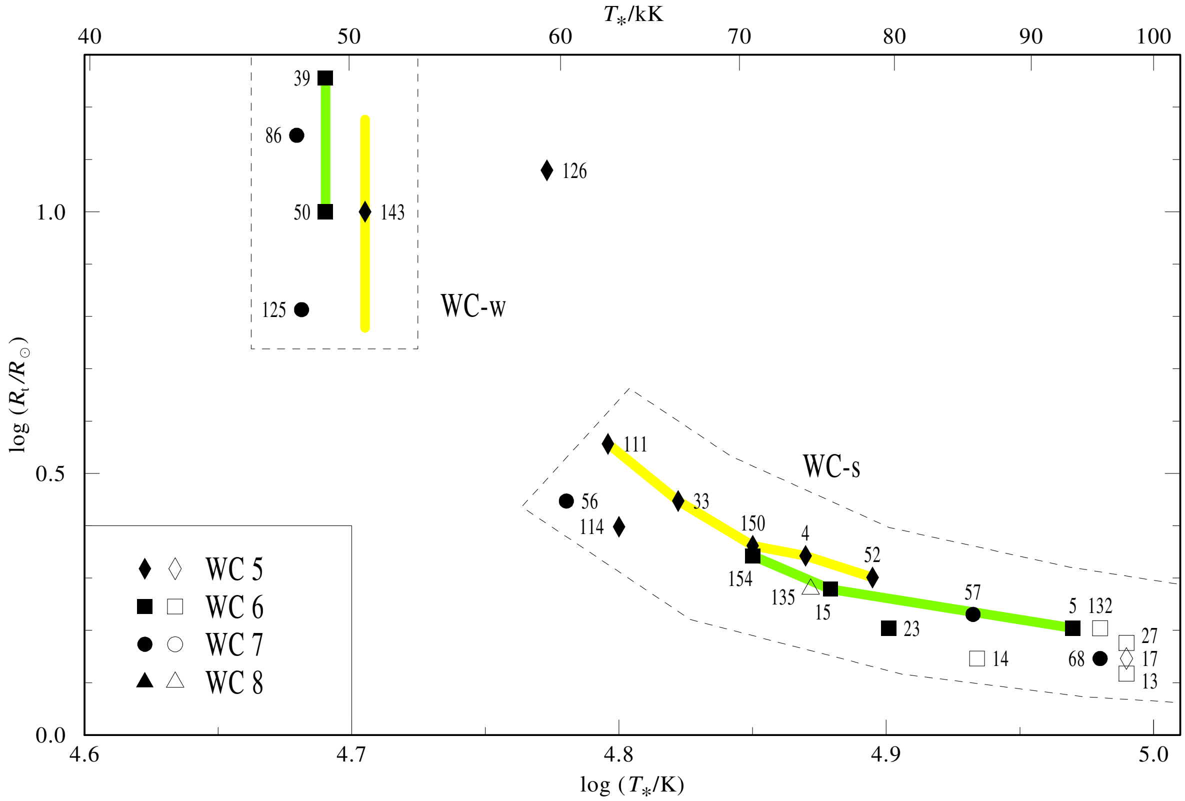

Fig. 16. Analyzed WC stars in the log T_*-log R_t-plane. The individual stars are labeled by their WR number. Stars with poor fit quality are represented by open symbols. The typical locations of WC 5 and WC 6 stars are suggested by shaded lines. Two groups can be clearly distinguished. The stars with weak lines (WC-w) have large transformed radii and relatively low stellar temperatures ($T_* \approx 50$ kK). Within their small temperature range the WC-w stars form a temperature sequence with higher temperatures for earlier subtypes. Only WR 126 has a considerably higher temperature than the other WC-w stars, but may be assigned to this group. The group of stars with strong lines (WC-s) form a narrow strip in the T_*-R_t-plane extending from T_* = 60 kK and R_t = 3.1 $R_\odot$ to T_* = 100 kK and R_t = 1.2 $R_\odot$. Within that strip the WC-s stars of later subtypes have a lower transformed radius, i.e. a higher wind density.

8.5. The Hertzsprung-Russell-Diagram

The HRD positions of the analyzed WC stars (diamonds) are shown in Fig. 19 together with the previously analyzed WN stars in our Galaxy (Hamann et al. 1993, 1994) and in the LMC (Koesterke et al. 1991). WC stars with known distance are emphasized by black symbols, because in the other cases (shaded diamonds) the luminosity depends on the M_v calibration which might introduce errors. Note that the symbols for WR 14 and WR 135 are also shaded since their analyses suffer from bad fit quality.

The WC-w stars form a vertical strip, similar to the WNE-w and WNL stars but at somewhat higher temperature. The WC-s stars populate a similar HRD region as the WNE-s stars, with T_* from 60 to 100 kK and log($L/L_\odot$) $\approx$ 4.9 ... 5.5. The WC 5 and WC 6 stars, especially the five stars with known distances, are crowding near the lower luminosity limit. The luminosities of the WC 7 stars are higher by 0.5 dex, typically.

8.6. The evolutionary status of the WR stars

The HRD positions of the WC stars are compared with theoretical predictions in Fig. 20. Only those five WC stars of our sample are shown (black diamonds) for which the results are most reliable (known distance and good fit quality; cf. Fig. 19). Furthermore, the Galactic WN stars analyzed by Hamann et al. (1993, 1994) are represented.

The evolutionary tracks shown for comparison were calculated within the standard scenario by Meynet et al. (1994) for solar metallicity (Z = 0.02). In contrast to previously released tracks of the same type (Schaller et al. 1992), the mass-loss rates are now assumed to be twice as large as the empirical values established for the pre-WR phases (cf. de Jager et al. 1988) and the WR phases.

For a wide range of initial masses ($\leq$ 85 $M_\odot$) the new tracks hardly differ from those of Schaller et al. (1992), but the evolution of the star with highest initial mass (120 $M_\odot$) changes drastically. This extremely massive star does not evolve at constant luminosities during the WNL phase as stars with smaller initial masses do, but fades from $10^{6.2}$ $L_\odot$ down to

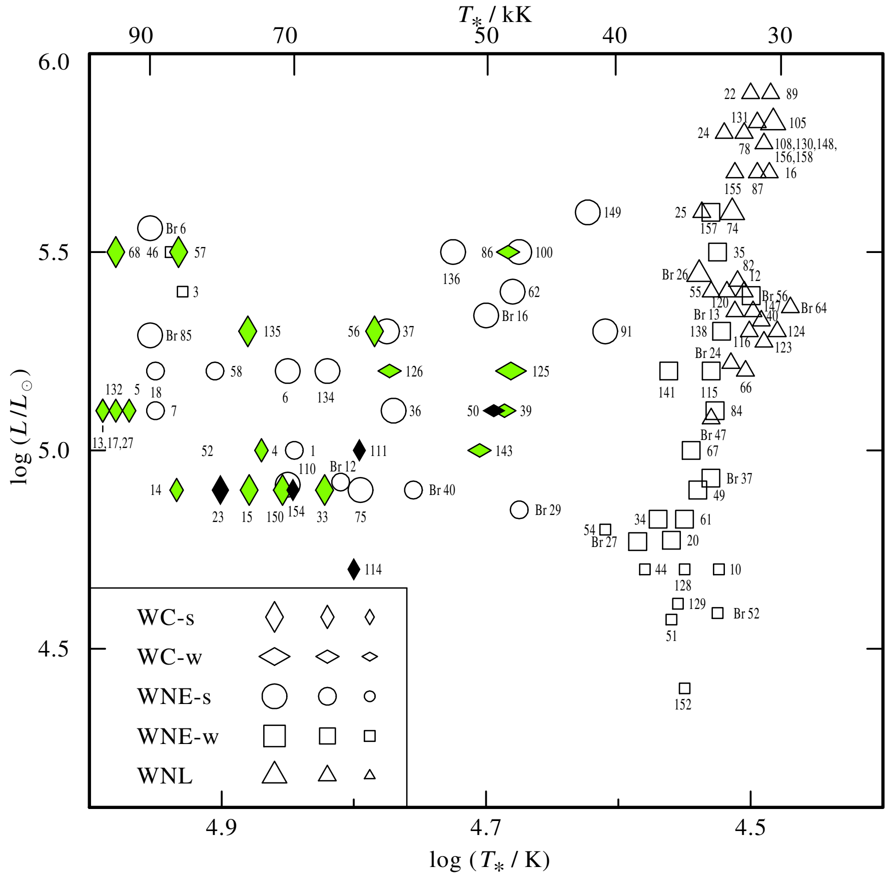

Fig. 19. HRD of Wolf-Rayet stars. The positions of the WC stars derived in the present paper are displayed together with the WN stars analyzed previously (Hamann et al. 1993, 1994; Koesterke et al. 1991 for LMC stars). The individual stars are identified by their WR and Br numbers, respectively (van der Hucht et al. 1988, Breysacher 1981). Those WC stars with known distance and analyses of good quality are represented by black diamonds while the other WC diamonds are shaded. The different sizes of the symbols indicate the mass-loss rate depending on whether $\log(\dot{M}/(M_\odot\,\mathrm{yr}^{-1}))$ is larger than -4.2 (large symbols), smaller than -4.8 (small symbols) or in between (medium size). The WC stars with weak lines (WC-w, horizontal diamonds) form a vertical strip at $T_* \approx 50$ kK, similar to the WNE-w and WNL stars which are arranged in a strip at 30 to 35 kK. The WC stars with strong lines (WC-s, vertical diamonds) populate a similar region as the early-type WN stars with strong lines (WNE-s), with T_* from 60 to 100 kK and luminosities of $10^{4.8}$ to $10^{5.5}$ $L_\odot$.

$10^{4.9}$ $L_\odot$. Consequently at final stages (WNE and WC) it is less luminous than stars of lower initial masses.

One problem which occurs when comparing evolutionary tracks with results of spectral analyses arises from the necessary definition of a reference radius for the effective temperature. The evolutionary models are in hydrostatic equilibrium, although real WR stars are obviously expanding in their outermost layers. The actual radii $R_{2/3}$ (defined by a Rosseland optical depth of 2/3) are certainly larger than predicted by equilibrium models, and hence the effective temperatures $T_{2/3}$ are lower. As the forces which make the WR stars unstable are not yet identified, there is no theoretical idea about how much the stellar radius is enlarged by the sub-photospheric acceleration. Any correction for this sub-photospheric extension (as e.g. proposed by Schaller et al. 1992) is necessarily based on arbitrary assumptions about the sub-photospheric velocity field.

By spectral analyses, on the other hand, only the visible layers of the stars can be investigated. Thus, only $R_{2/3}$ and $T_{2/3}$ can be considered as "observable" quantities, while R_* and T_* rely on the assumption that the adopted velocity law holds in subphotospheric layers as well. (Nevertheless, T_* is a useful parameter to distinguish the different groups of WR stars, cf. Fig. 19.)

Therefore, when comparing tracks and analyses in Fig. 20 we use as abscissa the effective temperatures referring to $R_{2/3}$ for the analyzed stars, but referring to the hydrostatic models for the theoretical tracks. Thus if stars look "cooler" than the corresponding track, this might not be considered as a contradiction, but as indication for a significant subphotospheric extension. Fig. 20 implies that the radii $R_{2/3}$ of the WC stars are actually about ten times larger than predicted by hydrostatic models.

Although the weak-lined WC stars (WC-w) have slightly higher $T_{2/3}$ than the WC-s stars (cf. Table 5), this removes only a minor part of the difference to the hydrostatic evolutionary models. Thus the enhanced radial extension is present in both groups, in the WC-w stars with thin winds as well as in the WC-s

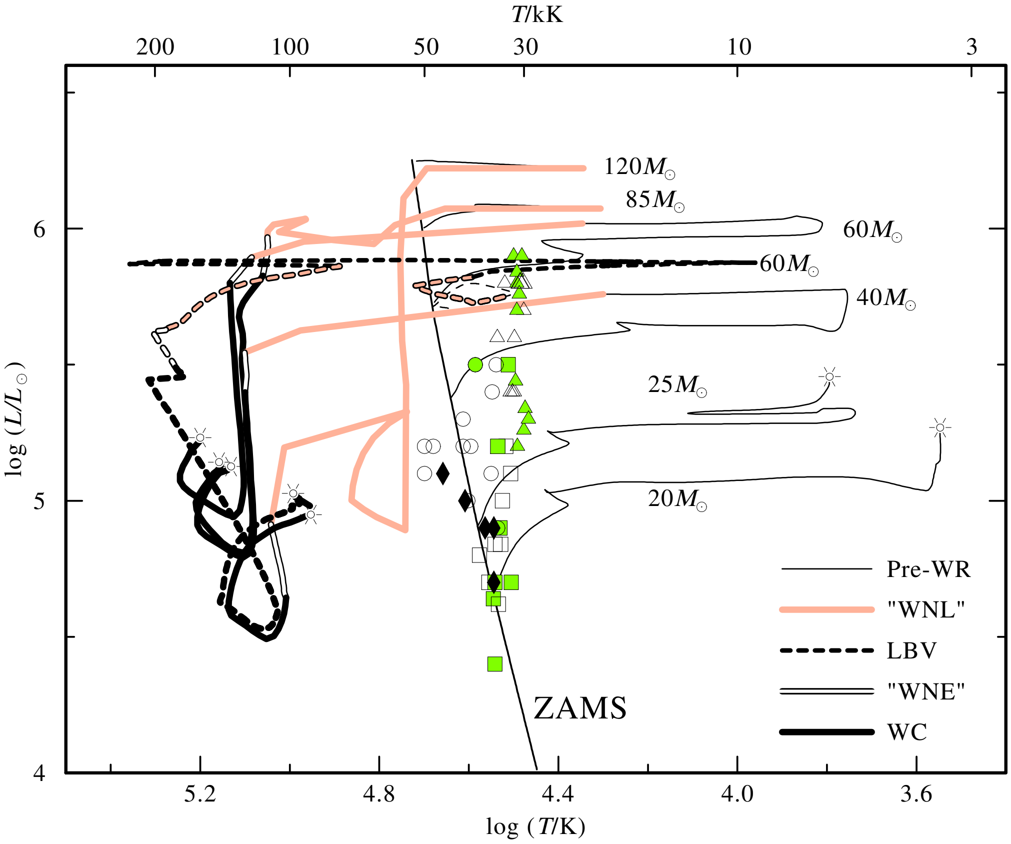

Fig. 20. HRD of WR stars and new standard evolutionary tracks from Meynet et al. (1994, solid lines). An alternative track from Langer et al. (1994, dashed lines) is additionally entered, which accounts for strong mass-loss caused by pulsational instabilities. The five WC stars with known distance and analyses of good fit quality are represented by black diamonds. The WN stars, previously examined by Hamann et al. (1993, 1994), are drawn by circles (WNE-s), squares (WNE-w) and triangles (WNL). The effective temperatures refer to the hydrostatic radius in case of the evolutionary tracks and to $R_{\tau=2/3}$ in case of the analyzed stars, respectively. Thus any differences in T are no contradiction but must be attributed to some subphotospheric extension of the stars (see text). Corresponding styles are used for stars and tracks. Shaded symbols denote a detectable hydrogen content in the atmospheres of WN stars and should be compared with the shaded "WNL" part of the tracks. Open symbols (WN stars without hydrogen) belong to the "WNE" tracks, while filled symbols (WC stars) correspond to the "WC" tracks (thick black line). The new tracks differ from previously released tracks by doubled mass-loss rates during all evolution stages. While most tracks (20 $M_\odot$ to 85 $M_\odot$) are hardly affected, the evolution of the most massive star (120 $M_\odot$) changes basically. The luminosity during the WNL phase drops drastically and the subsequent stages take place at very low luminosities. The observed WC luminosities are reached by various theoretical tracks. However, the low luminosities observed for the majority of WN stars are only reproduced by the 120 $M_\odot$ track which suffers from a dramatic decrease in luminosity during the WNL phase.

stars with strong winds. Hence this radius increase does not simlpy reflect that the lower parts of the wind become optically thick; it must be attributed to regions of very low velocities which are optically thick even in the case of relatively thin winds (WC-w).

Fig. 20 reveals that the empirical luminosities of the WC stars are covered by the theoretical tracks. Objections against the validity of the standard evolutionary calculations come from the WN stars (cf. Langer et al. 1994, Hamann 1994) and shall be only mentioned briefly here. The hydrogen abundances in WN stars are partly in conflict with the evolutionary predictions. Moreover, it seems unlikely that the majority of WR stars stems from progenitors as massive as 120 $M_\odot$. Finally, the doubling of the mass-loss rates applied in the evolutionary calculations is not supported from empirical facts.

An alternative evolutionary scenario has been proposed recently by Langer et al. (1994). Assuming that strong mass-loss caused by pulsational instabilities occurs already during the end of the core-hydrogen burning phase, an evolutionary sequence O $\rightarrow$ Of $\rightarrow$ H-rich WN $\rightarrow$ LBV $\rightarrow$ H-poor WN $\rightarrow$ H-free WN $\rightarrow$ WC $\rightarrow$ SN is predicted. A variety of observational facts which are in conflict with standard evolutionary models can be qualitatively explained by this new scenario. For the final WC stage, however, it predicts similar HRD positions as the standard tracks discussed here. Thus the present WC analyses provide no specific test between the two evolutionary scenarios.

Almost independently from their evolutionary past, WC stars should obey a mass-luminosity relation (Langer 1989). The typical WC luminosity of $10^{4.9}$ $L_\odot$ implies WC masses of 6

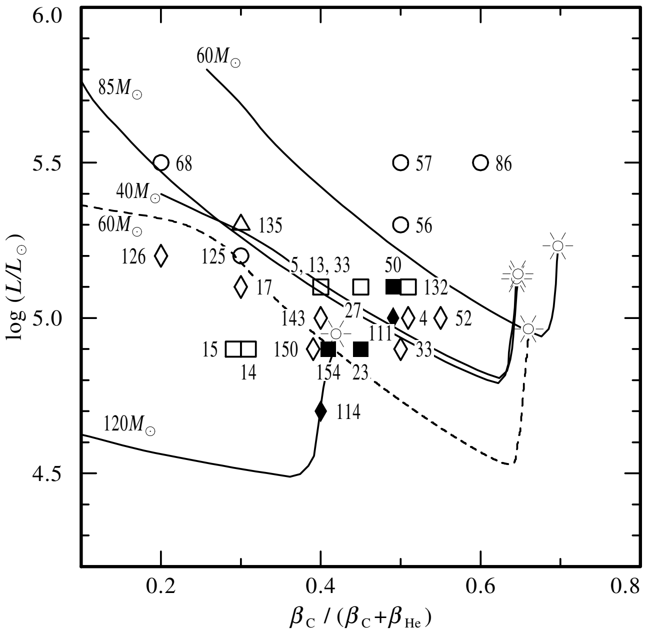

Fig. 21. Observed and predicted luminosities versus carbon mass fraction. The tracks for WC stars are taken from Meynet et al. (1994, solid lines) and from Langer et al. (1994, dashed lines). Because oxygen is neglected in our analyses, we have nomalized $\beta_C^{\rm Tracks}$ correspondingly. The stars evolve towards higher carbon mass fractions. The tracks of Meynet et al. (1994) with initial masses of 40 to 85 $M_\odot$ and the track from Langer et al. (1994) generally agree with the observed carbon mass fractions. The WR stars are represented by different symbols as explained in Fig. 16.

to 7 $M_\odot$, while the highest luminosities encountered ($10^{5.5}\,L_\odot$) yield up to 17 $M_\odot$.

For both evolutionary scenarios we compare the predicted carbon mass fraction with the results of our analyses (Fig. 21). The comparision must take into account that oxygen is neglected in our models. Therefore we have related the predicted carbon abundances from the evolutionary tracks to the total mass of helium and carbon (cf. Fig. 21). The tracks from Meynet et al. (1994) for initial masses from 40 to 85 $M_\odot$ generally agree with our empirical results. The highest carbon abundances at the end of the evolution, i.e. shortly before the SN explosion, might correspond to the earliest WC and WO subtypes which are not considered here. The 120 $M_\odot$ track does not lie in the observed $\beta_C - L$-domain. Note that this track is the only tracks from Meynet et al. (1994) which would explain the low WN luminosities observed. The alternative track ($M_{\rm ZAMS}$ = 60 $M_\odot$, with pulsation driven mass-loss) from Langer et al. (1994) also fits well.

8.7. Future work

We plan to extend our analyses of WC stars to the earliest (WC 4, WO) and latest (WC 9, WC 10) subtypes in order to complete the Galactic sample. The inclusion of oxygen into the models, which is mandatory for the earliest subtypes anyhow, will allow to determine oxygen abundances and hence provide further constraints on massive star evolution. Further insights are expected from studying WR stars in nearby galaxies, i.e. in environments with different metallicities. As an urgent improvement of the model atmospheres, the standard assumption of homogeneity must be replaced by some treatment of density fluctuations ("clumping").

Acknowledgements. L.K. acknowledges support from the Deutsche Forschungsgemeinschaft under grant Ha 1455/4-2. The calculations have been performed on the CRAY X-MP 216 of the Rechenzentrum der Universität Kiel and on the CRAY X-MP 216 and Y-MP 2E264 of the Konrad-Zuse-Zentrum für Informationsverarbeitung in Berlin.

References

Barlow M.J., Hummer D.G., 1982, in: Wolf-Rayet Stars: Observations, Physics, Evolution, eds. C.W.H. de Loore and A.J. Willis, IAU Symp. 99, p. 387

Breysacher J., 1981, A&AS 43, 203

Crowther P.A., Hillier D.J., Smith L.J., 1994a, A&A (in press)

Crowther P.A., Smith L.J., Hillier D.J., Schmutz W., 1994b, A&A (in press)

Eenens P.R.J, Williams P.M, 1992, MNRAS 255, 227

van Genderen A.M., Verheijen M.A.W., van Kampen E., 1991 in *Wolf-Rayet Stars and interrelations with other Massive Stars in Galaxies*, K.A. van der Hucht, B. Hidayat (eds), Proc. IAU Symp. 143, p.129

Hamann W.-R., 1994, in *Wolf-Rayet Stars: Binaries, Colliding Winds, Evolution*, K.A. van der Hucht, P.M. Williams (eds), Proc. IAU Symp. 163 (submitted)

Hamann W.-R., Leuenhagen U., Koesterke L., Wessolowski U., 1992, A&A 255, 200

Hamann W.-R., Koesterke L., Wessolowski U., 1993, A&A 274, 397

Hamann W.-R., Koesterke L., Wessolowski U., 1994, A&A (submitted)

Hillier D.J., 1988, ApJ 327, 822
Hillier D.J., 1989, ApJ 347, 392
Hillier D.J. 1991, in: Stellar Atmospheres: Beyond Classical Models, eds. L. Crivellari, I. Hubeny and D.G. Hummer, NATO ASI Series C, Vol. 341, p. 317
Howarth I.D., Schmutz W., 1992 A&A 261, 503
Hucht K.A., Conti P.S., Lundström I., Stenholm B., 1981, *Space Sci. Rev.* 28, 227
van der Hucht K.A., Hidayat B., Admiranto A., Supelli K.R., Doom C., 1988, A&A 199, 217
de Jager C, Nieuwenhuijzen H., van der Hucht K.A., 1988, A&AS 72, 259
Koesterke L., Hamann W.-R., Schmutz W., Wessolowski U., 1991, A&A 248, 166
Koesterke L., Hamann W.-R., Wessolowski U., 1992, A&A 261, 535
Kuhi L.V., 1968 in *Wolf-Rayet Stars,* K.B. Gebbie, R.N. Thomas (eds), NBS SP-307, p. 101
Langer N., 1989, A&A 210, 93
Langer N., Hamann W.-R., Lennon M., Najarro F., Pauldrach A.W.A., Puls J., 1994, A&A (in press)
Leuenhagen U., Hamann W.-R., 1994, A&A 283, 567
Meynet G., Maeder A., Schaller G., Schaerer D., Charbonnel C., 1994, A&AS 103, 97
Schaller G., Schaerer D., Meynet G., Maeder A., 1992, A&AS 96, 269
Schmutz W., Hamann W.-R., Wessolowski U., 1989, A&A 210, 236
Smith L.F., 1968, MNRAS 140, 409
Smith L.F., Hummer D.G., 1988, MNRAS 230, 511
Smith L.F., Maeder A., 1991, A&A 241, 77
Torres A.V., 1988 ApJ 325, 759
Torres A.V., Massey, P., 1987, ApJ Suppl. 65, 59
Torres A.V., Conti P.S., Massey P., 1986, ApJ 300, 379
Vreux J.-M., Andrillat Y., Biémont E., 1990 A&A 238, 207
Wessolowski U., Schmutz W., Hamann W.-R., 1988, A&A 194, 160

This article was processed by the author using Springer-Verlag LaTeX A&A style file *L-AA* version 3.